

$\bar{D}D$ meson pair production in antiproton-nucleus collisions

R. Shyam¹ and K. Tsushima²

¹*Saha Institute of Nuclear Physics, 1/AF Bidhan Nagar, Kolkata 700064, India and*

²*Laboratorio de Fisica Teorica e Computacional,
Universidade Cruzeiro do Sul, Rua Galvao Bueno,
868, Liberdade 01506-000, Sao Paulo, SP, Brazil*

(Dated: July 18, 2022)

Abstract

We study the $\bar{D}D$ (\bar{D}^0D^0 and D^-D^+) charm meson pair production in antiproton (\bar{p}) induced reactions on nuclei at beam energies ranging from threshold to several GeV. Our model is based on an effective Lagrangian approach that has only the baryon-meson degrees of freedom and involves the physical hadron masses. The reaction proceeds via the t -channel exchanges of Λ_c^+ , Σ_c^+ , and Σ_c^{++} baryons in the initial collision of the antiproton with one of the protons of the target nucleus. The medium effects on the exchanged baryons are included by incorporating in the corresponding propagators, the effective charm baryon masses calculated within a quark-meson coupling (QMC) model. The wave functions of the bound proton have been determined within the QMC model as well as in a phenomenological model where they are obtained by solving the Dirac equation with appropriate scalar and vector potentials. The initial- and final-state distortion effects have been approximated by using an eikonal approximation-based procedure. Detailed numerical results are presented for total and double differential cross sections for the \bar{D}^0D^0 and D^-D^+ production reactions on ^{16}O and ^{90}Zr targets. It is noticed that at \bar{p} beam momenta of interest to the $\bar{P}ANDA$ experiment, medium effects lead to noticeable enhancements in the charm meson production cross sections.

PACS numbers: 13.60.Le, 14.40.Lb, 11.10.Ef

I. INTRODUCTION

Several interesting and intriguing questions in hadron Physics can be elucidated by experiments involving medium-energy antiproton (\bar{p}) beam on fixed-targets. The future $\bar{P}ANDA$ (“antiproton annihilation at Darmstadt”) experiment at the underconstruction antiproton and ion Research facility (FAIR) at Darmstadt in Germany, will perform such studies at the beam momenta ≤ 15 GeV/c. The Physics program of $\bar{P}ANDA$ experiment [1] includes the study of bound states of quantum chromodynamics (QCD) up to the region of charm quarks. This will mainly concentrate on experiments on charmonium production, open charm spectroscopy, the search for charmed hybrids decaying to $\bar{D}D$, the rare decays and the charge-conjugation-parity (CP) violation in the D -meson sector. For accurate detection of the charmonium states above the $\bar{D}D$ threshold, reliable estimations are required for the production rates of \bar{D}^0D^0 and D^-D^+ meson pairs (to be together referred to as the $\bar{D}D$ mesons) in \bar{p} induced reactions on proton as well as heavier nuclear targets at the appropriate energies. The $\bar{P}ANDA$ experiment intends to carry out this task [2].

In a recent publication [3], calculations have been presented for the cross sections of the $\bar{p}+p \rightarrow \bar{D} + D$ reactions in the beam momentum range of threshold to 20 GeV/c within a single-channel effective Lagrangian model (ELM) (see, *e.g.*, Refs. [4–6]). In this approach, the dynamics of the production process is described by the t -channel Λ_c^+ , Σ_c^+ , and Σ_c^{++} baryon exchange diagrams. The initial- and final-state interactions have been accounted for by an eikonal type of phenomenological model. It has been found that at beam momenta beyond the threshold region, the total cross sections of the $\bar{p} + p \rightarrow \bar{D}^0 + D^0$ reaction are dominated by the contributions of the Λ_c^+ baryon exchange. These cross sections peak around $p_{\bar{p}}^{lab}$ of 9 GeV/c (with magnitudes close to $1 \mu\text{b}$). At $p_{\bar{p}}^{lab}$ around 15 GeV/c, which is of interest to the $\bar{P}ANDA$ experiment, the total cross section of this reaction as obtained in Ref. [3], is at least 5 times larger than its maximum value predicted in other studies [7–13]. The large \bar{D}^0D^0 production cross section raises the hope of studying the charm mixing, and searching for possible new physics contributions via clean signatures of charm CP violation [14].

On the other hand, in the ELM the $\bar{p} + p \rightarrow D^- + D^+$ reaction amplitudes involve only the Σ_c^{++} baryon exchange contribution. They have been found to be strongly suppressed compared to those of the \bar{D}^0D^0 production. This is attributed to the much smaller coupling constant of the Σ_c^{++} -exchange vertex in comparison to that of the Λ_c^+ -exchange. However, in the coupled-channels meson exchange model of Ref. [13], the initial state inelastic interactions could enhance the D^-D^+

production cross sections significantly.

The studies on the $\bar{D}D$ production in the \bar{p} -nucleus collisions are expected to explore the properties of the charm hadrons in nuclear medium and provide information about their interactions in the nuclear environment (see, e.g, a recent review [15]). The $\bar{P}ANDA$ experiment, with the capability of its detectors and the energy range of the storage ring, will be able to perform measurements for the cross sections of such reactions. The threshold momentum for $\bar{D}D$ production in \bar{p} induced reaction on proton is 6.40 GeV/c. This will be lowered in the \bar{p} reaction on nuclei due to the Fermi motion effects. Over the last years some efforts have been made to study theoretically the charm production in \bar{p} -nucleus reactions within a variety of models (see, e.g., Refs. [16–18]). The latter two studies concentrate on the calculations of the production of charmonium states J/Ψ and Ψ' . In Ref. [16], $\bar{D}D$ meson production in \bar{p} -nucleus reaction was investigated within a cascade model.

The aim of this paper is to study the \bar{D}^0D and D^-D^+ meson-pair productions in \bar{p} induced reactions on nuclei within an effective Lagrangian model. The basic production mechanism considered in our work is depicted in Fig. 1, where the $\bar{p} + A \rightarrow \bar{D} + D + B(= A - p)$ reactions proceed via t -channel Λ_c^+ , Σ_c^+ and Σ_c^{++} baryon exchange diagrams. The exchanges of both Λ_c^+ and Σ_c^+ baryons contribute to the amplitude of the $\bar{p} + A \rightarrow \bar{D}^0 + D^0 + B(= A - p)$ reaction. However, the $\bar{p} + p \rightarrow D^- + D^+ + B$ process is mediated only by the exchange of the Σ_c^{++} baryon. The t -channel part of our model is similar to that of the $\bar{p} + p \rightarrow \bar{D} + D$ reaction studied in Ref. [3]. It should be mentioned that the s -channel excitation, propagation and decay into the $\bar{D}D$ channels of the $\Psi(3770)$ resonance can also contribute to these reactions. In Ref. [3] it was shown that the contributions of the $\Psi(3770)$ resonance to the total cross sections of the $\bar{p} \rightarrow \bar{D}^0 + D^0$ reaction are insignificant at beam momenta away from the threshold region. Since our interest in this work is to estimate cross section at beam momenta of interest to the $\bar{P}ANDA$ experiment, we have not included such diagrams into our calculations.

In the next section we present our formalism where details of the ELM are presented and input required for making calculations within this model are discussed. The results and discussions of our work are given in Sec. III. Finally, the summary and conclusions of this study are presented in Sec. IV

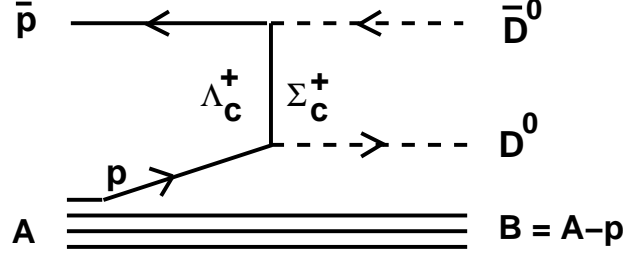


FIG. 1. Graphical representation of the model used to describe the $\bar{p} + A \rightarrow \bar{D}^0 + D^0 + B(= A - p)$ reaction via t -channel exchange of charmed baryons Λ_c^+ and Σ_c^+ . Similar representation applies also to the $\bar{p} + A \rightarrow D^- + D^+ + (A - p)$ reaction, but the intermediate line, in this case represents the exchange of Σ_c^{++} baryon.

II. FORMALISM

We have followed the procedure and notations of Ref. [19] in deriving the formulas for the invariant cross section of the $\bar{p} + A \rightarrow \bar{D} + D + B$ reaction, which can be written as (see, *e.g.*, Refs. [4, 20]),

$$d\sigma = \frac{m_{\bar{p}} m_A m_B}{\sqrt{[(p_{\bar{p}} p_A)^2 - m_{\bar{p}}^2 m_A^2]}} \frac{1}{4(2\pi)^5} \delta^4(P_f - P_i) |A_{fi}|^2 \times \frac{d^3 p_{\bar{D}}}{E_{\bar{D}}} \frac{d^3 p_D}{E_D} \frac{d^3 p_B}{E_B}, \quad (1)$$

where A_{fi} represents the total amplitude, P_i and P_f the sum of all the momenta in the initial and final states, respectively. $m_{\bar{p}}$, m_A and m_B are the masses of antiproton, and nuclei A and B, respectively. $p_{\bar{p}}$ and p_A are the momenta of the antiproton and the target nucleus, respectively. The cross sections in the laboratory or CM systems can be written from this equation by imposing the relevant conditions. Summations over final spin states and average over initial spin states are implied in $|A_{fi}|^2$.

To evaluate amplitudes for the processes represented in Fig. 1, we have used the effective Lagrangians at the charm baryon-meson-nucleon vertices, which are taken from Refs. [21–25]. For the vertices involved in the t -channel diagrams we have

$$\mathcal{L}_{NC_B D} = i g_{NC_B D} \bar{\psi}_N i \gamma^5 \phi_D \psi_{C_B} + H.c., \quad (2)$$

where ψ_N and ψ_{C_B} are the nucleon (antinucleon) and charmed baryon (C_B) fields, respectively, and ϕ_D is the D -meson field. $g_{NC_B D}$ in Eq. (2), represents the vertex coupling constant. For calculating

the amplitude of the processes (one of the two) represented in Fig. 1, we require the in-medium propagators for the intermediate baryons C_B (Λ_c^+ , Σ_c^+ , and Σ_c^{++}). We write these propagators as,

$$\mathcal{D}_{C_B}(q_{C_B}) = \frac{i(\gamma_\mu q_{C_B}^\mu + m_{C_B}^*)}{q_{C_B}^2 - (m_{C_B}^* - i\Gamma_{C_B}/2)^2}, \quad (3)$$

where we have introduced the effective mass of the charmed baryon, $m_{C_B}^*$, to take into account the medium effects on the propagation of the charmed baryon in the nuclear medium. In Eq. (3) q_{C_B} and Γ_{C_B} are the four-momentum and width of the exchanged charmed baryon, respectively. We have calculated $m_{C_B}^*$ within the quark-meson coupling (QMC) model [26], employing the QMC-I version of the model [27, 28]. The details of this calculation are given in section II.A. In the following, the free-space (vacuum) mass of the exchanged charmed baryon will be represented by m_{C_B} . For Λ_c^+ and Σ_c^+ charmed baryons, the values of m_{C_B} are taken to be 2285 MeV and 2452 MeV, respectively. The values of $m_{C_B}^*$ and m_{C_B} for Σ_c^{++} have been taken to be the same as those of Σ_c^+ .

In Eq. (3), we have taken the latest Particle Data Group estimates [29] for the width Γ_{C_B} . It should, however, be noted that the medium effects can also modify the widths of the exchange baryons (see, *e.g.*, Ref. [30]). Nevertheless, because making predictions for the modification in the widths of the charmed baryons is at present out of the scope of the QMC model, we continue to use on-shell widths for the exchanged baryons, which are very small in any case.

The amplitude of the process depicted in Fig. 1, is given by

$$A_{fi} = i \frac{g_{NC_B D}^2}{q_{C_B}^2 - (m_{C_B}^* - i\Gamma_{C_B}/2)^2} \bar{\psi}_{\bar{p}}(k_{\bar{p}}) \gamma^5 (\gamma_\mu q_{C_B}^\mu + m_{C_B}^*) \gamma^5 \psi_A(k_p), \quad (4)$$

where $\psi_A(k_p)$ is the spinor for the bound proton in the initial channel. It is a four component Dirac spinor, which is the solution of the Dirac equation for a bound state problem in the presence of external scalar and vector potential fields. This is written as (see, *e.g.*, Ref. [31])

$$\psi(k_p) = \delta(k_{p0} - E_p) \begin{pmatrix} f(K_p) \mathcal{Y}_{\ell 1/2 j}^{m_j}(\hat{k}_p) \\ -ig(K_p) \mathcal{Y}_{\ell' 1/2 j}^{m_j}(\hat{k}_p) \end{pmatrix}. \quad (5)$$

In our notation k_p represents a four momentum, and \mathbf{k}_p a three momentum. The magnitude of \mathbf{k}_p is represented by K_p , and its directions by \hat{k}_p . k_{p0} represents the time-like component of momentum k_p . In Eq. (5), $f(K_p)$ and $g(K_p)$ are the radial parts of the upper and lower components of the spinor $\psi(k_p)$, and $\mathcal{Y}_{\ell 1/2 j}^{m_j}$ represent the coupled spherical harmonics. The latter is given by

$$\mathcal{Y}_{\ell 1/2 j}^{m_j} = \langle \ell m_\ell 1/2 \mu_i | j m_j \rangle Y_{\ell m_\ell}(\hat{k}_p) \chi_\mu, \quad (6)$$

where $Y_{\ell m_\ell}$ represents the spherical harmonics, and χ_μ the spin-space wave function of a spin- $\frac{1}{2}$ particle. In Eq. (5) $\ell' = 2j - \ell$ with ℓ and j being the orbital and total angular momenta, respectively.

The coupling constants g_{NCBD} are adopted from Refs. [22, 23], as $g_{N\Lambda_c^+D} = 13.50$, $g_{N\Sigma_c^+D} = 2.69$ and $g_{N\Sigma_c^{++}D} = 2.69$. From these values it is expected that Λ_c^+ will dominate the t -channel production amplitudes.

The off-shell behavior of the vertices is regulated by a monopole form factor (see, e.g., Refs. [4, 5])

$$F_i(q_{C_{Bi}}) = \frac{\lambda_i^2 - m_{C_{Bi}}^{*2}}{\lambda_i^2 - q_{C_{Bi}}^2}, \quad (7)$$

where index i represent the i -th exchanged baryon. λ_i is the corresponding cutoff parameter, which governs the range of suppression of the contributions of high momenta carried out via the form factor. We chose a value of 3.0 GeV for λ_i at all the vertices. The same λ_i was also used in the monopole form factor employed in the studies of the $\bar{\Lambda}_c^-\Lambda_c^+$ and $\bar{D}D$ production in the $\bar{p}p$ collisions in Refs. [21] and [3], respectively, within a similar type of the effective Lagrangian model. Since our calculations are carried out in momentum space, they include all the nonlocalities in the production amplitudes that arise from the resonance propagators.

We have used plane waves to describe the motions of antiproton and \bar{D} meson in the entrance and outgoing channels, respectively. However, initial and final state interactions are approximately accounted for within an eikonal approximation based procedure (see section 2.B).

A. Effective charmed baryon mass in nuclear matter within the quark-meson coupling model

A relativistic effective Lagrangian density in QMC-I model for hypernuclei in mean field approximation, which is used for studying the in-medium modifications of charmed baryons and

production of charmed mesons (in a nucleus), is given by [32–38]:

$$\mathcal{L}_{QMC} = \mathcal{L}_{QMC}^N + \mathcal{L}_{QMC}^Y, \quad (8)$$

$$\begin{aligned} \mathcal{L}_{QMC}^N \equiv & \bar{\psi}_N(\mathbf{r}) \left[i\boldsymbol{\gamma} \cdot \partial - M_N^*(\sigma) - (g_\omega \omega(\mathbf{r}) + g_\rho \frac{\tau_3^N}{2} b(\mathbf{r}) + \frac{e}{2}(1 + \tau_3^N)A(\mathbf{r}))\gamma_0 \right] \psi_N(\mathbf{r}) \\ & - \frac{1}{2}[(\nabla\sigma(\mathbf{r}))^2 + m_\sigma^2\sigma(\mathbf{r})^2] + \frac{1}{2}[(\nabla\omega(\mathbf{r}))^2 + m_\omega^2\omega(\mathbf{r})^2] \\ & + \frac{1}{2}[(\nabla b(\mathbf{r}))^2 + m_\rho^2 b(\mathbf{r})^2] + \frac{1}{2}(\nabla A(\mathbf{r}))^2, \end{aligned} \quad (9)$$

$$\begin{aligned} \mathcal{L}_{QMC}^Y \equiv & \bar{\psi}_Y(\mathbf{r}) \left[i\boldsymbol{\gamma} \cdot \partial - M_Y^*(\sigma) - (g_\omega^Y \omega(\mathbf{r}) + g_\rho^Y I_3^Y b(\mathbf{r}) + eQ_Y A(\mathbf{r}))\gamma_0 \right] \psi_Y(\mathbf{r}), \\ & (Y = \Lambda, \Sigma^{0,\pm}, \Xi^{0,+}, \Lambda_c^+, \Sigma_c^{0,+}, \Xi_c^{0,+}, \Lambda_b), \end{aligned} \quad (10)$$

where $\psi_N(\mathbf{r})$ and $\psi_Y(\mathbf{r})$ are the nucleon and the hyperon (strange, charm or bottom baryon) fields, respectively.

In an approximation where the σ , ω and ρ fields couple only to the u and d light quarks, the coupling constants for the hyperon Y , are obtained as $g_\omega^Y = (n_q/3)g_\omega$, and $g_\rho^Y \equiv g_\rho = g_\rho^q$, with n_q being the total number of valence light quarks in the hyperon Y . I_3^Y and Q_Y are the third component of the hyperon isospin operator and its electric charge in units of the proton charge, $|e|$, respectively. The field dependent σ - N and σ - Y coupling strengths, $g_\sigma(\sigma) \equiv g_\sigma^N(\sigma)$ and $g_\sigma^Y(\sigma)$, appearing in Eqs. (9) and (10), are defined by

$$M_N^*(\sigma) \equiv M_N - g_\sigma(\sigma)\sigma(\mathbf{r}), \quad (11)$$

$$M_Y^*(\sigma) \equiv M_Y - g_\sigma^Y(\sigma)\sigma(\mathbf{r}), \quad (12)$$

where M_N (M_Y) is the free nucleon (hyperon) mass. Note that the dependence of these coupling strengths on the applied scalar field must be calculated self-consistently within the quark model [26, 27, 33, 34, 39, 40]. Hence, unlike quantum hadro dynamics (QHD) model [41], even though $g_\sigma^Y(\sigma)/g_\sigma(\sigma)$ may be 2/3 or 1/3 depending on the number of light quarks in the hyperon in free space, $\sigma = 0$ (even this is true only when their bag radii in free space are exactly the same), this will not necessarily be the case in a nuclear medium.

In the following, we consider the limit of infinitely large, uniform (symmetric) nuclear matter, where all scalar and vector fields become constant. In this limit, we can treat any single hadron (denoted by h) embedded in the nuclear medium in the same way as we treated a hyperon. One simply need to replace \mathcal{L}_{QMC}^Y in Eq. (10) by the corresponding Lagrangian density for the hadron h .

The Dirac equations for the quarks and antiquarks ($q = u$ or d , and $Q = s, c$ or b , hereafter) in the bag of hadron h in nuclear matter at the position $x = (t, \mathbf{r})$ are given by [42, 43]:

$$\left[i\boldsymbol{\gamma} \cdot \partial_x - (m_q - V_\sigma^q) \mp \gamma^0 \left(V_\omega^q + \frac{1}{2} V_\rho^q \right) \right] \begin{pmatrix} \psi_u(x) \\ \psi_{\bar{u}}(x) \end{pmatrix} = 0, \quad (13)$$

$$\left[i\boldsymbol{\gamma} \cdot \partial_x - (m_q - V_\sigma^q) \mp \gamma^0 \left(V_\omega^q - \frac{1}{2} V_\rho^q \right) \right] \begin{pmatrix} \psi_d(x) \\ \psi_{\bar{d}}(x) \end{pmatrix} = 0, \quad (14)$$

$$[i\boldsymbol{\gamma} \cdot \partial_x - m_Q] \psi_Q(x) \text{ (or } \psi_{\bar{Q}}(x)) = 0, \quad (|\mathbf{r}| \leq \text{bag radius}), \quad (15)$$

where we neglect the Coulomb force, and assume SU(2) symmetry for the light quarks ($q = u = d$). The constant mean-field potentials in nuclear matter are defined by, $V_\omega^q \equiv g_\omega^q \omega$ and $V_\rho^q \equiv g_\rho^q b$, with g_σ^q , g_ω^q and g_ρ^q the corresponding quark-meson coupling constants. Note that $V_\rho^q = 0$ in symmetric nuclear matter, although this is not true in a nucleus where the Coulomb force induces the proton and neutron distribution asymmetry even in a nucleus with the same numbers of protons and neutrons to give, $V_\rho^q \propto (\rho_p - \rho_n) \neq 0$ at a given position in a nucleus.

The normalized, static solution for the ground state quarks or antiquarks with flavor f in the hadron h , may be written as, $\psi_f(x) = N_f e^{-i\epsilon_f t / R_h^*} \psi_f(\mathbf{r})$, where N_f and $\psi_f(\mathbf{r})$ are the normalization factor and the corresponding spin and spatial part of the wave function, respectively. The bag radius in medium for a hadron h (R_h^*) is determined through the stability condition for the mass of the hadron against the variation of the bag radius [26, 27, 40]. The eigenenergies in units of $1/R_h^*$ are given by,

$$\begin{pmatrix} \epsilon_u \\ \epsilon_{\bar{u}} \end{pmatrix} = \Omega_q^* \pm R_h^* \left(V_\omega^q + \frac{1}{2} V_\rho^q \right), \quad \begin{pmatrix} \epsilon_d \\ \epsilon_{\bar{d}} \end{pmatrix} = \Omega_q^* \pm R_h^* \left(V_\omega^q - \frac{1}{2} V_\rho^q \right), \quad \epsilon_Q = \epsilon_{\bar{Q}} = \Omega_Q. \quad (16)$$

The hadron masses in a nuclear medium m_h^* (free mass m_h), are calculated by

$$m_h^* = \sum_{j=q, \bar{q}, Q, \bar{Q}} \frac{n_j \Omega_j^* - z_h}{R_h^*} + \frac{4}{3} \pi R_h^{*3} B, \quad \left. \frac{\partial m_h^*}{\partial R_h} \right|_{R_h=R_h^*} = 0, \quad (17)$$

where $\Omega_q^* = \Omega_{\bar{q}}^* = [x_q^2 + (R_h^* m_q^*)^2]^{1/2}$, with $m_q^* = m_q - g_\sigma^q \sigma$, $\Omega_Q^* = \Omega_{\bar{Q}}^* = [x_Q^2 + (R_h^* m_Q)^2]^{1/2}$, and $x_{q,Q}$ being the lowest bag eigen frequencies. $n_q(n_{\bar{q}})$ and $n_Q(n_{\bar{Q}})$ are the quark (antiquark) numbers for the quark flavors q and Q , respectively. The MIT bag quantities, z_h , B , $x_{q,Q}$, and $m_{q,Q}$ are the parameters for the sum of the c.m. and gluon fluctuation effects, bag constant, lowest eigenvalues for the quarks q or Q , respectively, and the corresponding current quark masses. z_N

TABLE I. Current quark masses (input), coupling constants and the bag constant.

| | | | |
|-----------|----------|--------------|---------|
| $m_{u,d}$ | 5 MeV | g_σ^q | 5.69 |
| m_s | 250 MeV | g_ω^q | 2.72 |
| m_c | 1300 MeV | g_ρ^q | 9.33 |
| m_b | 4200 MeV | $B^{1/4}$ | 170 MeV |

TABLE II. The bag parameters, various hadron masses and the bag radii in free space [at normal nuclear matter density, $\rho_0 = 0.15 \text{ fm}^{-3}$] z_h, R_h and M_h [M_h^* and R_h^*]. M_h and $R_N = 0.8$ fm in free space are inputs.

| h | z_h | M_h (MeV) | R_h (fm) | M_h^* (MeV) | R_h^* (fm) |
|-------------|-------|-------------|------------|---------------|--------------|
| N | 3.295 | 939.0 | 0.800 | 754.5 | 0.786 |
| Λ_c | 1.766 | 2284.9 | 0.846 | 2162.5 | 0.843 |
| Σ_c | 1.033 | 2452.0 | 0.885 | 2330.2 | 0.882 |

and $B(z_h)$ are fixed by fitting the nucleon (the hadron) mass in free space. For the current quark masses we use $(m_{u,d}, m_s, m_c, m_b) = (5, 250, 1300, 4200)$ MeV, where the values for m_c and m_b are the averaged values from Refs. [44] and [45], respectively, and these values were used in Refs. [35–38]. Since, the effects of the bare quark mass values used are very small on the results, we use the same values as used in the past so that we can compare and discuss the results with those obtained previously [35–38]. This also applies for the baryon mass values used. The bag constant calculated for the present study is $B = (170 \text{ MeV})^4$. The quark-meson coupling constants, which are determined so as to reproduce the saturation properties of symmetric nuclear matter (the binding energy per nucleon of 15.7 MeV at $\rho_0 = 0.15 \text{ fm}^{-3}$), are $(g_\sigma^q, g_\omega^q, g_\rho^q) = (5.69, 2.72, 9.33)$, where $g_\sigma \equiv g_\sigma^N \equiv 3g_\sigma^q S_N(0) = 3 \times 5.69 \times 0.483 = 8.23$ [39]. These are summarized in Table I. The parameters z_h , and the bag radii R_h for relevant baryons in free space, and some quantities calculated at normal nuclear matter density $\rho_0 = 0.15 \text{ fm}^{-3}$ are listed in Table II, together with the free space masses (inputs) [44–47].

In Fig. 2 (a), we show the effective masses of the charmed baryons C_B , and in Fig. 2 (b) the scalar potentials in symmetric nuclear matter as a function of nuclear density. We note that $m_{C_B}^* \leq m_{C_B}$ at finite density as usually expected. The attractive mass-shift that reflects the reduced

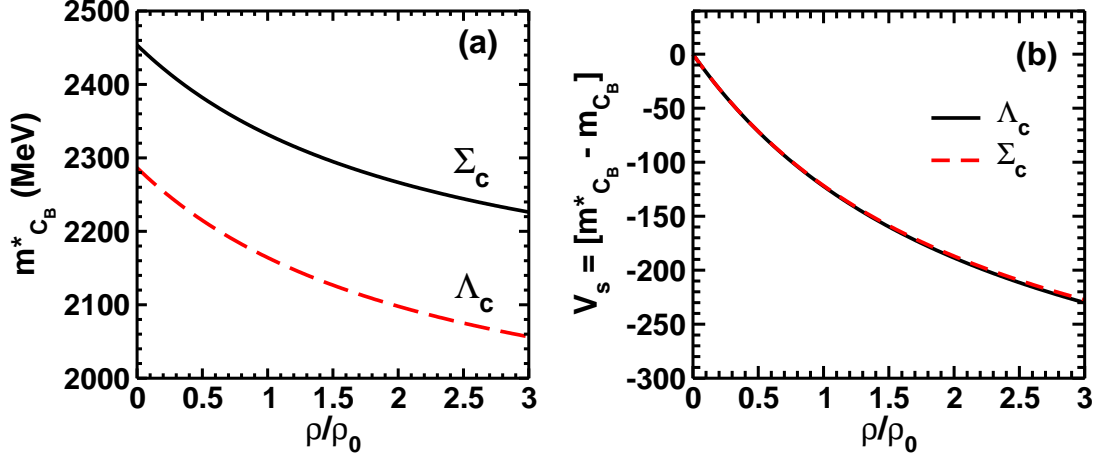


FIG. 2. [Color online] (a) Effective masses of the charmed baryons Λ_c^+ and Σ_c^+ in symmetric nuclear matter as a function of matter density, as calculated within the QMC-I model. (b) Scalar potential for Λ_c^+ and Σ_c^+ charmed baryons as a function of a matter density in symmetric nuclear matter.

light-quark condensates at finite density, have been predicted for vector mesons as well [48, 49], although the issues of in-medium widths related with the collision broadening must be studied carefully in the experimental situations. Our calculations predict the similar observation for the charm baryon sector as those for the strange sector and the nucleons. We further note that in-medium mass shift of charmed baryons leads to an attractive scalar potential of about 120.00 MeV at normal nuclear matter density $\rho = \rho_0$.

B. Initial- and final-state interactions

From the studies of the $\bar{\Lambda}_c^- \Lambda_c^+$ and $\bar{D} D$ production [3, 21, 50] in the $\bar{p} p$ collisions, it was found that the magnitudes of the cross sections depend very sensitively on the initial-state distortion effects. In fact, the $\bar{p} p$ annihilation channel is almost as strong as the elastic scattering channel. Consequently, in \bar{p} -nucleus reactions also these distortion effects are expected to be as significant. They can produce both absorptive as well as dispersive effects. However, for large incident energies involved in this study, the absorptive effects are likely to be most important. We estimate these within an eikonal approximation, as discussed below.

Within the eikonal approximation, the attenuation factor for a particle traveling through the nuclear medium can be written as (see, e.g. Ref. [31])

$$S(E) = \int d\mathbf{b} dz \frac{\rho(\mathbf{b}, z) \exp[-k \eta_0(E) L(b)]}{\int d\mathbf{b} dz \rho(\mathbf{b}, z)}, \quad (18)$$

where η_0 is the imaginary part of the refractive index of the nuclear medium and $\rho(r)[\rho(\sqrt{b^2 + z^2})]$ is the nuclear density distribution, with b being the impact parameter. In Eq. (18) $L(b)$ is the length of the path traveled by the particle in the medium, which is given by

$$L(b) = \int_0^\infty \frac{\rho(r)}{\rho_0} dz. \quad (19)$$

If the nuclear density is approximated by a Gaussian function, $\rho(r) = \rho_0 \exp(-r^2/\alpha^2)$, the integration in Eq. (18) can be done analytically. In this case the attenuation factor is given by

$$S(E) = \frac{1 - \exp[-\sqrt{\pi} \alpha k \eta_0(E)]}{\sqrt{\pi} \alpha k \eta_0(E)}. \quad (20)$$

The attenuation due to medium can be calculated if the value of $\eta_0(E)$ is known. This can be obtained from the imaginary part of the optical potential W_0 as

$$\eta_0(E) = \frac{1}{\hbar^2} \frac{E}{k^2} W_0(E). \quad (21)$$

One can use the following high energy relations to relate W_0 to the $\bar{p}p$ total cross section, σ_T

$$W_0(E) = \hbar^2 \frac{k \sigma_T \rho_0}{2E}. \quad (22)$$

In order to determine the total reduction factor for the $\bar{p} + A \rightarrow \bar{D}^0 + D^0 + B (= A - p)$ reaction, the total attenuation due to both the antiproton and D -meson distortions has been estimated by replacing the factor $k\eta_0$ in Eq. (20) by

$$k\eta_0 \rightarrow k_{\bar{p}}\eta_0(E_{\bar{p}}) + k_{\bar{D}}\eta_0(E_{\bar{D}}) + k_D\eta_0(E_D). \quad (23)$$

The information about the \bar{p} -nucleus imaginary potential is not very firm [51, 52] particularly at higher beam momenta of interest to the $\bar{P}ANDA$ experiment. In our estimation of the attenuation we have taken the average value of the imaginary part of the \bar{p} -nucleus optical potential to be 125 MeV, which is in agreement with the values reported in Refs. [53, 54] at higher antiproton momenta. We have made this value independent of the beam momentum and the target nucleus. This corresponds to a $\bar{p}p \sigma_T$ of about 75 mb at \bar{p} momentum of 15 GeV/c², with a ρ_0 of 0.15 fm⁻³. This value is somewhat larger than those reported in Refs. [55] and [56].

At the same time, the knowledge about the \bar{D} - and D -nucleus potentials is extremely scarce. We have taken a value of 10 mb for $\bar{D}N$ and $DN \sigma_T$ [56, 57]. The value of the parameter α is taken to be 2.73 fm and 4.30 fm for ¹⁶C and ⁹⁰Zr targets, respectively [58].

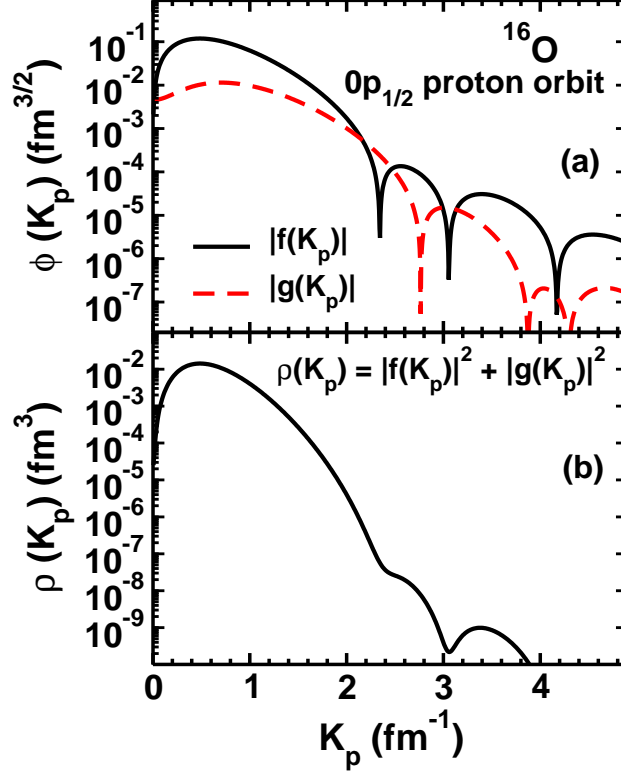


FIG. 3. (color online) (a) Momentum space spinors ($\phi(K_p)$) for $0p_{1/2}$ nucleon orbit in ^{16}O . $f(K_p)$ and $g(K_p)$ are the upper and lower components of the spinor, respectively. (b) Momentum distribution ($\rho(K_p)$) for the same state calculated with the wave function shown in (a).

III. RESULTS AND DISCUSSIONS

The initial bound proton spinors (corresponding to momenta K_p) are required to perform numerical calculations of the amplitudes in Eq. (4). To simplify the nuclear structure problems, we assume the bound proton states to have a pure single particle-hole configuration (with the core remaining inert), having quantum numbers of the outermost proton orbit of the target nucleus, even though it is straightforward to include also those cases where the participating proton occupies other orbits. This corresponds to the $0p_{1/2}$ orbit with a binding energy of 12.13 MeV in case of the ^{16}O target, and the $1p_{1/2}$ orbit with a binding energy of 8.35 MeV for ^{90}Zr target.

The spinors in the momentum space are obtained by Fourier transformation of the corresponding coordinate space spinors, which are the solutions of the Dirac equation with potential fields consisting of an attractive scalar part and a repulsive vector part having a Woods-Saxon form. This choice appears to be justified as the Dirac Hartree-Fock calculations [59, 60] suggest that these

TABLE III. Searched depths of vector and scalar potentials and the binding energies of the nucleon bound states.

| State | Binding Energy (ϵ) (MeV) | V_s (MeV) | r_s (fm) | a_s (fm) | V_v (MeV) | r_v (fm) | a_v (fm) |
|----------------------------|--|----------------|---------------|---------------|----------------|---------------|---------------|
| $^{16}\text{O}(0p_{1/2})$ | 12.13 | -445.56 | 0.983 | 0.606 | 360.91 | 0.983 | 0.606 |
| $^{90}\text{Zr}(1p_{1/2})$ | 8.35 | -418.55 | 0.983 | 0.606 | 339.03 | 0.983 | 0.606 |

potentials tend to follow the nuclear shape.

In the phenomenological model, the potential fields were obtained by a well-depth searched procedure. In this method, with fixed geometry parameters (radius and diffuseness), the depths of the scalar (V_s) and (V_v) potentials are searched to reproduce the binding energies of the respective proton bound states with the given choice of quantum numbers. For the target nuclei, ^{16}O , and ^{90}Zr , the resulting values are shown in Table I. To show the momentum spread of the corresponding spinors, we have displayed in Figs. 3 and 4, the spinors $|f(K_p)|$ and $|g(K_p)|$ and the momentum distribution $\rho(K_p) = |f(K_p)|^2 + |g(K_p)|^2$ as a function of momentum K_p for ^{16}O and ^{90}Zr targets, respectively. It was shown in Ref. [61] that spinors calculated in this way provide a good description of the nucleon momentum distribution for the p shell nucleons. We note that in the region of momentum transfer pertinent to charm-meson production in \bar{p} -nucleus collisions, the lower components of the spinors are not negligible as compared to the upper component, which clearly demonstrates that a fully relativistic approach is essential for an accurate description of this reaction.

The bound state spinors have also been calculated within the QMC-I model (see, *e.g.*, Ref. [62]). Even though the binding energies of the bound proton orbitals predicted by the QMC model were somewhat different from those used in the fitting procedure of the phenomenological model, the spinors obtained in two models were almost identical to each other.

Using the formalism, approximations and the input parameters given in section II and the bound state spinors described above, we have investigated the $\bar{D}^0 D^0$ and $D^- D^+$ production in the \bar{p} collision with a light ($A = ^{16}\text{O}$) and a medium mass ($A = ^{90}\text{Zr}$) nucleus. We emphasize that parameters like coupling constants at the vertices and the shapes of the form factors and the values of the cut-off parameters involved therein, were the same as those used in the studies of the $\bar{D}^0 D^0$ and

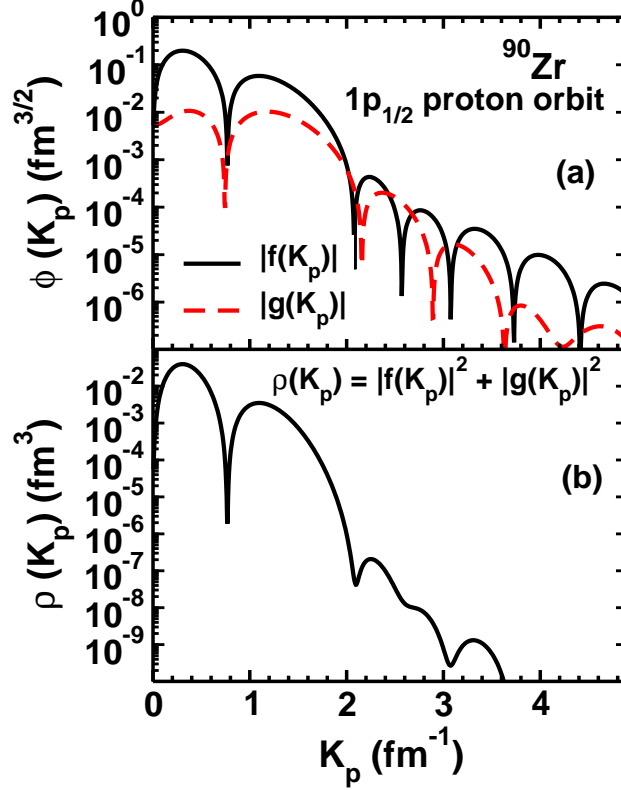


FIG. 4. (color online) (a) Momentum space spinors ($\phi(K_p)$) for $1p_{1/2}$ nucleon orbit in ^{90}Zr . $f(K_p)$ and $g(K_p)$ are the upper and lower components of the spinor, respectively. (b) Momentum distribution ($\rho(K_p)$) for the same state calculated with the wave function shown in (a).

D^-D^+ charmed meson productions in the $\bar{p}p$ collisions at the beam momenta ranging from the corresponding threshold to 20 GeV/c in Refs. [3] and [21], respectively. In each case the effects of initial- and final-state interactions are included by following the procedure described in section II.B.

In Fig. 5, we display the beam momentum dependence of the cross section $d\sigma/d\Omega_{\bar{D}^0}$ at $\theta_{\bar{D}^0} = 0^\circ$ for the $\bar{p} + {}^{16}\text{O} \rightarrow \bar{D}^0 + D^0 + {}^{15}\text{N}$ reaction. In this figure the arrow shows the threshold for the \bar{D}^0D^0 production in $\bar{p}p$ collision, which is 6.4 GeV/c. In contrast, the thresholds of this reaction on ${}^{16}\text{O}$ and ${}^{90}\text{Zr}$ targets are 2.89 GeV/c and 2.68 GeV/c, respectively. The shift in the threshold of \bar{p} -nucleus reactions is mainly due to Fermi motion effects.

The solid line in Fig. 5 shows the cross section obtained by using in the reaction amplitudes the in-medium effective mass ($m_{C_B}^*$) of the exchanged charmed baryon (ECB) that are calculated self-consistently within the QMC-I model as discussed in section II.A. The dotted line represents the results obtained with the free-space (vacuum) mass (m_{C_B}) for ECB. It is clear that at the \bar{p} beam

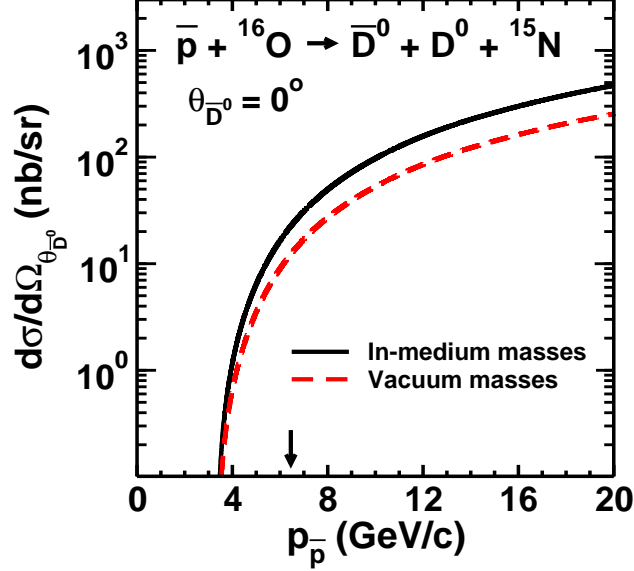


FIG. 5. (color online) Differential cross section $d\sigma/d\Omega_{\bar{D}^0}$ at $\theta_{\bar{D}^0} = 0^\circ$ as function of antiproton beam momentum for the reaction $\bar{p} + {}^{16}\text{O} \rightarrow \bar{D}^0 + D^0 + {}^{15}\text{N}$. The results obtained with the in-medium effective mass ($m_{C_B}^*$) of the exchanged charm-baryons are shown by the full line, while those with the free-space (vacuum) mass m_{C_B} are represented by the dashed line. In both cases the contributions of Λ_c^* and Σ_c^* (intermediate states) are coherently summed in the reaction amplitude.

momenta ($p_{\bar{p}}$) of interest to the $\bar{P}ANDA$ experiment (around 15 GeV/c), the effect of nuclear medium is noticeable. In this region the cross sections calculated with the effective mass $m_{C_B}^*$ of ECB are about a factor of two larger than those obtained with the vacuum mass m_{C_B} .

In the amplitudes corresponding to the cross sections shown in Fig. 5, the individual contributions of the Λ_c^+ and Σ_c^+ exchanges have been coherently summed. However, we have noted that these cross sections are almost solely governed by the Λ_c^+ -exchange mechanism in the entire range of the antiproton beam momentum. The contributions of Σ_c^+ -exchange terms are lower by about 3 orders of magnitudes. This reflects the trend seen in the case of $\bar{D}^0 D^0$ production in $\bar{p}p$ collisions in Ref. [3]. This can be understood from the fact that the coupling constants of the vertices involved in the Σ_c^+ -exchange are much smaller than those of the Λ_c^+ -exchange.

In Fig. 6, we show the cross sections $d\sigma/d\Omega_{D^+}$ at $\theta_{D^+} = 0^\circ$ for the $\bar{p} + {}^{16}\text{O} \rightarrow D^- + D^+ + {}^{15}\text{N}$ reaction as a function of \bar{p} beam momentum. We see that in this case the cross sections are strongly suppressed compared to those of Fig. 5. The cross sections of the $\bar{p} + p \rightarrow D^- + D^+$ reactions also were found to be similarly suppressed as compared to those of the $\bar{p} + p \rightarrow \bar{D}^0 + D^0$ reaction in Ref. [3] where calculations were performed within a similar ELM model. Same trend

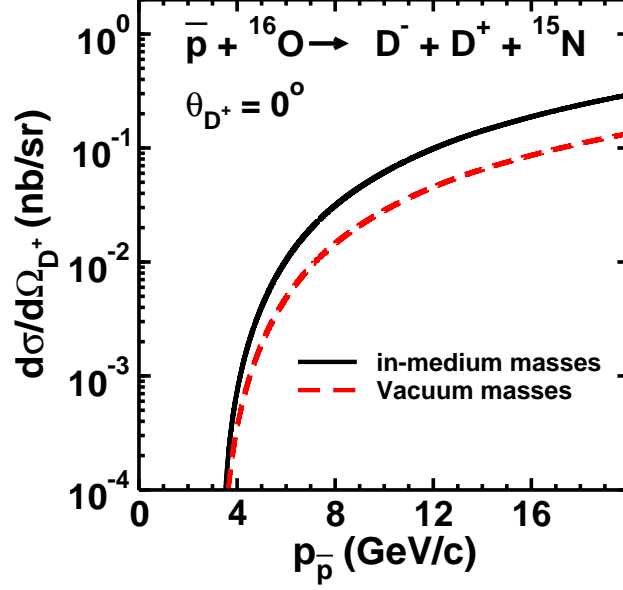


FIG. 6. (color online) Differential cross section $d\sigma/d\Omega_{D^+}$ at $\theta_{D^+} = 0^\circ$ as function of antiproton beam momentum for the reaction $\bar{p} + {}^{16}\text{O} \rightarrow D^- + D^+ + {}^{15}\text{N}$. The solid and dashed lines have the same meaning as in Fig. 5.

was also observed in the calculations presented in Refs. [7–9] within models that use the idea of Regge trajectory-exchange. In both the cases, this effect can be understood from the fact that while the $\bar{D}^0 D^0$ production is dominated by the Λ_c^+ -exchange mechanism, the $D^- D^+$ production gets contributions only from the Σ_c^{++} -exchange terms. The coupling constants in the latter case have been taken to be equivalent to those of the Σ_c^+ -exchange vertices. Therefore, they are much smaller than those of the Λ_c^+ -exchange terms. The ratio of the absolute magnitudes of the $\bar{D}^0 D^0$ and $D^- D^+$ production cross sections is roughly proportional to $(g_{N\Lambda_c^+ D}/g_{N\Sigma_c^{++} D})^4$, which leads to a reduction in the $D^- D^+$ production cross section over that of $\bar{D}^0 D^0$ by nearly a factor of 650.

However, in the coupled-channels meson-exchange model of Ref. [13], the $\bar{p} + p \rightarrow D^- + D^+$ cross sections are even larger than the $\bar{p} + p \rightarrow \bar{D}^0 + D^0$ ones. This results from their coupled-channels treatment of the incident channel, which accounts effectively for two-step inelastic processes involving Λ_c^+ "baryon exchange". Such two-step mechanisms are out of the scope of our ELM as well as of the Regge model [7–9] calculations. Therefore, in studies within these models the $D^- D^+$ production is suppressed as compared to the $\bar{D}^0 D^0$ production reaction. It should be mentioned here that the cross sections for the $\bar{p} + p \rightarrow D^- + D^+$ reaction from Ref. [13] were used as input in Ref. [57] in the calculations of the formation cross sections of the D -mesic nucleus

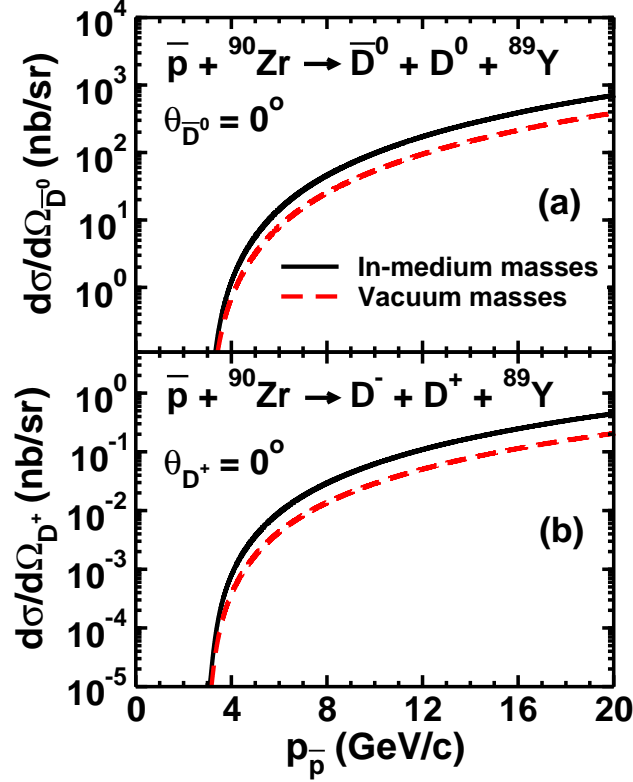


FIG. 7. (color online) (a) Differential cross section $d\sigma/d\Omega_{\bar{D}^0}$ at $\theta_{\bar{D}^0} = 0^\circ$ as function of antiproton beam momentum for the reaction $\bar{p} + {}^{90}\text{Zr} \rightarrow \bar{D}^0 + D^0 + {}^{89}\text{Y}$. The results obtained with the in-medium effective mass ($m_{C_B}^*$) of the exchanged charm-baryons are shown by the full line while those with the free-space mass m_{C_B} by the dashed line. (b) Differential cross section $d\sigma/d\Omega_{D^+}$ at $\theta_{D^+} = 0^\circ$ as function of antiproton beam momentum for the reaction $\bar{p} + {}^{90}\text{Zr} \rightarrow D^- + D^+ + {}^{89}\text{Y}$. The solid and dashed lines have the same meaning as in Fig. 7(a).

$[{}^{11}\text{B}-D^-]$ via the reaction $\bar{p} + {}^{12}\text{C} \rightarrow [{}^{11}\text{B}-D^-] + D^+$ within a Green's function method. The magnitudes of the formation cross sections predicted in Ref. [57] will be strongly suppressed if our cross sections for the $\bar{p} + p \rightarrow D^- + D^+$ reaction are used as input.

The solid and dashed lines in Fig. 6 correspond to calculations performed with the effective in-medium mass $m_{C_B}^*$ and the vacuum mass m_{C_B} , respectively. We see that for this reaction too, for $p_{\bar{p}}$ around 15 GeV/c, the cross section obtained with the in-medium mass $m_{C_B}^*$ are larger than those obtained with m_{C_B} by about a factor of two.

In Fig. 7(a) and 7(b), we display the cross sections $d\sigma/d\Omega_{\bar{D}^0}$ at $\theta_{\bar{D}^0} = 0^\circ$ for the $\bar{p} + {}^{90}\text{Zr} \rightarrow \bar{D}^0 + D^0 + {}^{89}\text{Y}$ reaction, and $d\sigma/d\Omega_{D^+}$ at $\theta_{D^+} = 0^\circ$ for the $\bar{p} + {}^{90}\text{Zr} \rightarrow D^- + D^+ + {}^{89}\text{Y}$ reaction, respectively, as a function of $p_{\bar{p}}$. The solid and dashed lines have the same meaning as those in

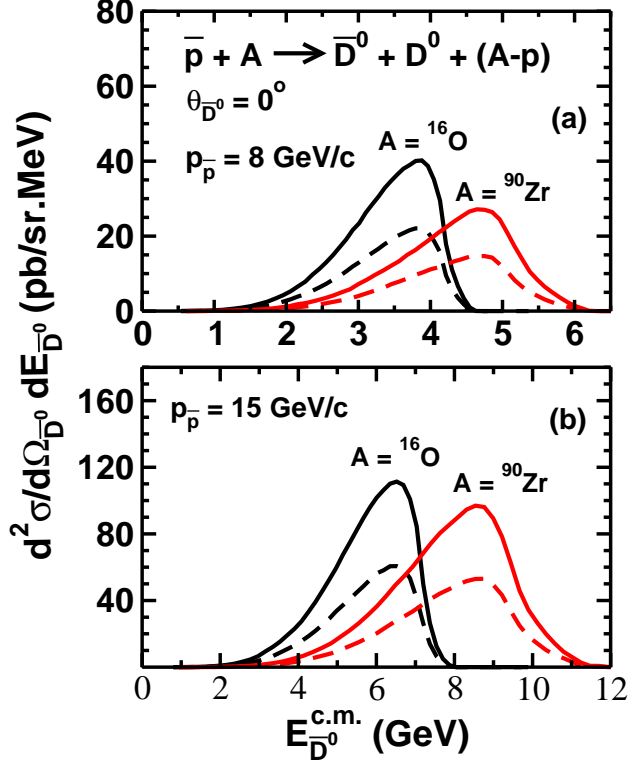


FIG. 8. (color online) (a) Double differential cross section $d^2\sigma/d\Omega_{\bar{D}^0}dE_{\bar{D}^0}$ at $\theta_{\bar{D}^0} = 0^\circ$ for the $\bar{p} + A \rightarrow \bar{D}^0 + D^0 + (A-p)$ reaction where $A = {}^{16}\text{O}$ and ${}^{90}\text{Zr}$, as a function of \bar{D}^0 energy $E_{\bar{D}^0}$ at the \bar{p} beam momentum of 8 GeV/c. The solid and dashed lines represent the results obtained with the in-medium effective charmed-baryon mass and the free-space charmed baryon mass, respectively. (b) The same as in Fig. 8(a) but at the \bar{p} beam momentum of 15 GeV/c.

Figs. 5 and 6. We note that all the features of the cross sections that were observed in case of the reactions on the lighter ${}^{16}\text{O}$ target are also present in those on this medium mass target. There is, however, one difference. While the cross sections on the ${}^{90}\text{Zr}$ and ${}^{16}\text{O}$ targets are approximately similar for $p_{\bar{p}} \leq 10$ GeV/c, they start differing from each other for $p_{\bar{p}} \geq 10$ GeV/c. In this region the cross section on the heavier target becomes gradually larger than those on the lighter one.

In Figs. 8(a) and 8(b), we present the results for the double differential cross section $d^2\sigma/d\Omega_{\bar{D}^0}dE_{\bar{D}^0}$ at $\theta_{\bar{D}^0} = 0^\circ$ for the $\bar{D}^0 D^0$ production in \bar{p} induced reaction on ${}^{16}\text{O}$ and ${}^{90}\text{Zr}$ targets at $p_{\bar{p}}$ of 8 GeV/c and 15 GeV/c, respectively, as a function of the center-of-mass (c.m.) energy, $E_{\bar{D}^0}^{c.m.}$, of \bar{D}^0 charmed-meson. The solid and the dashed lines represent the results obtained by using masses $m_{C_B}^*$ and m_{C_B} , respectively, for the ECB in the calculations. It is seen that these cross sections are peaked very close to the maximum allowed values of $E_{\bar{D}^0}^{c.m.}$ ($E_{\bar{D}^0}^{c.m.,max}$) corresponding to the given target

and the beam momentum. This effect is found for reactions on both the targets. As the target mass increases, $E_{D^0}^{c.m.,max}$ shifts to higher values so does the peak position in the corresponding cross section. The widths of the distributions are somewhat larger for the heavier target.

Although the effect of using the in-medium effective mass of the exchanged charmed-baryon is visible in the entire \bar{D}^0 energy spectrum, this is more prominent in the region around the peak position, where peak cross sections obtained by using in-medium mass $m_{C_B}^*$ in the amplitude are larger by nearly a factor of two than those obtained with the free-space mass m_{C_B} .

Therefore, future measurements of the $\bar{D}D$ production in \bar{p} induced reactions on nuclei to be performed with the $\bar{P}ANDA$ detector at the FAIR facility are expected to provide a handle to probe the in-medium properties of the charmed-baryons.

Finally we acknowledge that a major source of uncertainty of our results is provided by our treatment of the initial- and final-state interactions. We account for these effects within an eikonal-approximation-based phenomenological method. Although, the parameters of our method ($\bar{p}N$ total cross section and the radius parameter of the target nuclei) can be checked from the independent sources, they should ideally be constrained by fitting to the experimental data. Because of the lack of any experimental information, it is not yet possible to test our model thoroughly. Thus the absolute magnitudes of our cross sections may have some uncertainties. Furthermore, in the present treatment we considered the absorptive distortion effects only that influence the absolute magnitudes of the cross sections. In a more rigorous treatment, the inclusion of dispersive effects may affect the shapes of the cross sections also.

IV. SUMMARY AND CONCLUSIONS

In Summary, we have studied the production of charmed-meson pairs \bar{D}^0D^0 and D^-D^+ in antiproton induced reactions on ^{16}O and ^{90}Zr targets by using a single-channel effective Lagrangian model that involves meson-baryon degrees of freedom. The dynamics of the production process is described by the t-channel diagrams involving exchanges of charmed baryons Λ_c^+ , Σ_c^+ , and Σ_c^{++} during the collision between the antiproton and a proton bound in the target. The initial- and final-state interactions have been taken into account by an eikonal type of phenomenological model. The coupling constants at the charmed-baryon exchange vertices were taken to be the same as those used in the studies of $\bar{p} + p \rightarrow \bar{D} + D$ and $\bar{p} + p \rightarrow \bar{\Lambda}_c^- + \Lambda_c^+$ reactions in Refs. [3] and [21], respectively. These coupling constants were deduced in Ref. [23] from the analysis of the DN and

$\bar{D}N$ scatterings. The same coupling constants were also used for the vertex couplings involved in the D -meson-nucleon interactions in the studies reported in Ref. [22]. The off-shell corrections at various vertices have been accounted for by introducing monopole form factors with the cut-off parameters having the same value as those used in our studies reported in Refs. [21] and [3]. It is a general practice, however, to determine the shape of the form factors and the cut-off parameters involve therein by fitting to the experimental data. Because, such data are not yet available for the reactions under study in this paper, we restricted ourselves to the choice of the form factor and the cut-off parameter that were used in our previous study of this reaction on a proton target. The bound proton spinors have been obtained by solving the Dirac equation with vector and scalar potential fields having Woods-Saxon shapes. Their depths are fitted to the binding energy of the respective state.

We find that the differential cross sections for the production of $\bar{D}^0 D^0$ charmed-meson pair at the \bar{D}^0 angle of 0° in \bar{p} induced reaction on both ^{16}O and ^{90}Zr targets, are dominated by the contributions of the Λ_c^+ baryon exchange - the Σ_c^+ -exchange contributions are quite small due to relatively smaller coupling constants. The cross sections of the $D^- D^+$ production that gets contributions solely from the Σ_c^{++} baryon exchange process, are strongly suppressed due the smaller coupling constants of the corresponding vertices.

The double differential cross sections for the $\bar{p} + A \rightarrow \bar{D}^0 + D^0$ reaction for observing \bar{D}^0 at 0° have maxima in the vicinity of the kinematically allowed maximum values of \bar{D}^0 c.m. energies. This feature is independent of the \bar{p} beam momentum and the target mass. The widths of the corresponding spectra are, however, target-mass dependent.

A significant result of our study is that using in-medium effective masses in the propagators of the exchanged charmed baryons leads to about a factor two increase in the cross sections at most forward angle over those obtained with the corresponding free-space masses, for antiproton beam momenta around 8-15 GeV/c, which are of interest to the $\bar{P}ANDA$ experiment. This result is independent of the mass of the target nucleus. This observation suggests that in-medium properties of the charmed baryon may be experimentally accessible in this experiment.

V. ACKNOWLEDGMENTS

This work has been supported by the Science and Engineering Research Board (SERB), Department of Science and Technology, Government of India under grant no. SB/S2/HEP-024/2013,

and Fundação de Amparo à Pesquisa do Estado de São Paulo (FAPESP), Brazil, no. 2016/04191-3, and, no. 2015/17234-0, and Ministério da Ciência, Tecnologia, Inovações e Comunicações (CNPq), no. 400826/2014-3, and, no. 308088/2015-8.

- [1] W. Erni *et al.*, arXiv:0903.3905.
- [2] O. N. Hartmann *et al.*, Int. J. Mod. Phys. A **22**, 578 (2007).
- [3] R. Shyam and H. Lenske, Phys. Rev. D **93**, 034016 (2016).
- [4] R. Shyam, Phys. Rev. C **60**, 055213 (1999).
- [5] R. Shyam and U. Mosel, Phys. Rev. C **67**, 065202 (2003).
- [6] R. Shyam, O. Scholten and A. W. Thomas, Phys. Rev. C **84**, 042201 (R) (2011).
- [7] A. B. Kaidalov and P. E. Volkovitsky, Z. Phys. C **63**, 517 (1994).
- [8] A. Khodjamirian, Ch. Klein, Th. Mannel, and Y.-M. Wang, Eur. Phys. J. A **48**, 31 (2012).
- [9] A. I. Titov and B. Kämpfer, Phys. Rev. C **78**, 025201 (2008).
- [10] A. T. Goritschnig, B. Pire and W. Schweiger, Phys. Rev. D **87**, 014017 (2013); Phys. Rev. D **88**, 079903(E) (2013).
- [11] A. T. Goritschnig, P. Kroll, and W. Schweiger, Eur. Phys. J. A **42**, 43 (2009).
- [12] P. Kroll, B. Quadder, and W. Schweiger, Nucl. Phys. **B316**, 373 (1989).
- [13] J. Haidenbauer, and G. Krein, Phys. Rev. D **89**, 114003 (2014).
- [14] D. H. Kaplan, Nucl. Phys. A **844**, 206 (2010).
- [15] Laura Tolos, EPJ Web of Conferences, **97**, 00027 (2015).
- [16] A. Sibirtsev, K. Tsushima and A. W. Thomas, Eur. Phys. J. **6**, 351 (1999).
- [17] L. Gerland, L. Frankfurt and M. Strikmann, Phys. Lett. B **619**, 95 (2005).
- [18] A. B. Larionov, M. Bleicher, A. Gillitzer and M. Strikman, Phys. Rev. C **87**, 054608 (2013)
- [19] J. D. Bjorken and S. D. Drell, *Relativistic Quantum Mechanics* (McGraw-Hill, New York, 1964).
- [20] R. Shyam, O. Scholten and A.W. Thomas, Phys. Rev. C **88**, 025209 (2013).
- [21] R. Shyam and H. Lenske, Phys. Rev. D **90**, 014017 (2014).
- [22] T. J. Hobbs, J. T. Londergan, and W. Melnitchouk, Phys. Rev. D **89**, 074008 (2014)
- [23] J. Haidenbauer, G. Krein, U.-G. Meissner, and L. Tolos, Eur. Phys. J. A **47**, 18 (2011).
- [24] A. Müller-Groeling, K. Holinde, and J. Speth, Nucl. Phys. **A513**, 557 (1990).
- [25] J. Van de Wiele and S. Ong, Eur. Phys. J. A **46**, 291 (2010).

- [26] P. A. M. Guichon, Phys. Lett. B **200**, 235 (1988)
- [27] P. A. M. Guichon, K. Saito, E. N. Rodionov, and A. W. Thomas, Nucl. Phys. A **601**, 349 (1996).
- [28] K. Saito, K. Tsushima and A. W. Thomas, Nucl. Phys. A **609**, 339 (1996).
- [29] K. A. Olive *et al.* (Particle Data Group), Chin. Phys. C **38**, 090001 (2014).
- [30] S. Leuopold, V. Metag and U. Mosel, Int. J. Mod. Phys. E **19**, 147 (2010).
- [31] R. Shyam, H. Lenske and U. Mosel, Nucl. Phys. A **764**, 313 (2006).
- [32] K. Saito, K. Tsushima, A.W. Thomas, Prog. Part. Nucl. Phys. **58**, 1 (2007).
- [33] K. Tsushima, K. Saito, A.W. Thomas, Phys. Lett. B **411**, 9 (1997); *ibid.* **421**,413 (1998) (E).
- [34] K. Tsushima, K. Saito, J. Haidenbauer, A.W. Thomas, Nucl. Phys. A **630**, 691 1998.
- [35] K. Tsushima, F.C. Khanna, Phys. Lett. B **552**, 138 (2003).
- [36] K. Tsushima, F.C. Khanna, Phys. ReV. C **67**, 015211 (2003).
- [37] K. Tsushima, F.C. Khanna, Prog. Theor. Phys. **149**, 160 (2003).
- [38] K. Tsushima, F.C. Khanna, J. Phys. G **30**, 1765 (2004).
- [39] K. Saito, K. Tsushima, and A.W. Thomas, Nucl. Phys. A **609**, 339 (1996).
- [40] K. Saito and A.W. Thomas, Phys. Lett. B **327**, 9 (1994).
- [41] B.D. Serot and J.D. Walecka, Adv. Nucl. Phys. **16**, 1 (1986).
- [42] K. Tsushima, K. Saito, A.W. Thomas, S.V. Wright, Phys. Lett. B **429**, 239 (1998); *ibid.* **436**, 453 (1998)(E)
- [43] K. Tsushima, D.H. Lu, A.W. Thomas, K. Saito, R.H. Landau, Phys. Rev. C **59**, 2824 (1999).
- [44] (PDG96) R.M. Barnett *et al.*, Phys. Rev. D **54**, 1 (1996).
- [45] D.E. Groom *et al.*, Eur. Phys. J. C **15**, 1 (2000).
- [46] C. Caso *et al.*, Eur. Phys. J. C **3**, 1 (1998).
- [47] K. Hagiwara *et al.*, Phys. Rev. D **66**, 010001 (2002).
- [48] G. E. Brown and M. Rho, Phys. Rev. Lett. **66**, 2720 1991.
- [49] T. Hatsuda and S. H. Lee, Phys. Rev. C **46**, 34 (1992).
- [50] J. Haidenbauer, and G. Krein, Phys. Lett. B **687**, 314 (2010).
- [51] T. Gaitanos, M. Kaskulov and H. Lenske, Phys. Lett. B **703**, 193 (2011).
- [52] J. Hrtankova and J. Mares, Nucl. Phys. A **945**, 197 (2016).
- [53] Zhang Yu-shun, Liu Ji-feng, B. A. Robson, and Li Yang-guo, Phys. Rev. C **54**, 332 (1996).
- [54] A. B. Larionov and H. Lenske, arXiv:1609.03343 [nucl-th].
- [55] J. Haidenbauer, G. Krein, U.-G. Meissner and A. Sibirtsev, Eur. Phys. J. A **37**, 55 (2008).

- [56] Teck-Ghee Lee and Cheuk-Yin Wong, Phys. Rev. C **89**, 054601 (2014).
- [57] J. Yamagata-sekihara, C. Garcia-Recio, J. Nieves, L. L. Salcedo, and L. Tolos, Phys. Lett. B **754**, 26 (2016)
- [58] R. C. Barrett and D. F. Jackson, *Nuclear Sizes and Structure*, (Oxford, 1977).
- [59] L. D. Miller and A. E. S. Green, Phys. Rev. C **5**, 241 (1972).
- [60] R. Brockmann, Phys. Rev. C **18**, 1510 (1978).
- [61] R. Shyam, W. Cassing and U. Mosel, Nucl. Phys. **A586** (1995) 557.
- [62] R. Shyam, K. Tsushima, and A. W. Thomas, Nucl. Phys. A **881**, 255 (2012).